HTML ABSTRACT + LINKS

Condensation phenomena in nanopores: A Monte Carlo study

Raja Paul[a] and Heiko Rieger
Theoretische Physik, Universität des Saarlandes, 66041 Saarbrücken, Germany

(Received 23 December 2004; accepted 9 June 2005; published online 20 July 2005)

The nonequilibrium dynamics of condensation phenomena in nanopores is studied via Monte Carlo simulations of a lattice-gas model. Hysteretic behavior of the particle density as a function of the density of a reservoir is obtained for various pore geometries in two and three dimensions. The shape of the hysteresis loops depend on the characteristics of the pore geometry. The evaporation of particles from a pore can be fitted to a stretched exponential decay of the particle density. Phase-separation dynamics inside the pore is effectively described by a random walk of the nonwetting phases. Domain evolution is significantly slowed down in the presence of a random wall-particle potential and gives rise to a temperature-dependent growth exponent. A geometric roughness of the pore wall only delays the onset of a pure domain growth. © *2005 American Institute of Physics*. [DOI: 10.1063/1.1993554]

I. INTRODUCTION

Adsorption and desorption isotherms of a gas condensed into nanopores show hysteresis and have become a very useful tool for the classification of porous materials.[1–3] Due to the effect of surface tension the formation of meniscii inside the pore is delayed on the desorption branch, resulting in a nonvanishing hysteresis area of the sorption isotherms. A theoretical analysis and detailed description of the early research on this phenomenon is described in a review by Everett.[4] A recent investigation from a point of view of the stability of adsorbed multilayers[5] and other[6–8] analytical and numerical approaches together with density-functional theory also proposed that the hysteresis phenomenon is an intrinsic property of the phase transition in a single-idealized pore and arises from the existence of metastable states. Although real nanoporous materials consist of an interconnected network of simple pores,[9,10] quite recently it has been shown by numerical analysis[11] and experiments[12–14] that hysteresis can occur in isolated pores also. Moreover the shape of the hysteresis loops are influenced by the characteristic features of the pore geometry.

In this paper we try to get an insight into the nonequilibrium dynamics in general and the adsorption/desorption hysteresis, in particular, within a single nanopore—on the basis of a microscopic model. Using extensive Monte Carlo simulations, we intend to characterize the sorption isotherms for different pore geometries and compare our results directly to the experimental observations. Moreover we try to get an insight into the mechanism for the extremely slow dynamics in the confined geometry of a single pore during adsorption and desorption processes as well as during domain growth. We study the phase-separation kinetics of a binary liquid in nanopores at low temperatures. The demixing transition of a binary fluid within a solid gel has been investigated in Ref. 15. Other works[16–18] showed that a binary liquid, unlike Ising-type complete phase separation, does not separate into two phases completely. Instead the adsorbed material forms many small domains far inside the coexistence region.

It has been suggested that this behavior is a consequence of a random pore geometry and can be understood on the basis of the random-field Ising model (RFIM).[19–21] However, Monette *et al.*[22] argued that this picture does not apply to Vycor, with much lower porosity than gels. These are the systems we are interested in and we focus mainly on isolated (single) pores with a homogeneous wall-particle potential—and will consider the effect of periodicity in the wall structure and randomness in the wall-particle potentials at the end of our work.

A very slow segregation dynamics (as also predicted within the RFIM picture) takes place in single pores without randomness because the confinement in a small pore slows down domain growth in certain regions of the wetting phase diagram[22] and as a result macroscopic phase separation is not observed on short-time scales. Moreover, the late-stage domain evolution, obtained from a two point correlation function $C(r,t)$, follows the same Lifshitz-Slyozov[23] growth law of $t^{1/3}$. Unlike earlier works[24] on domain evolution in porous networks, we concentrate on a single pore which is more applicable for systems with low porosity (Si mesopores[14]). Randomness in terms of an irregular pore structure or presence of impurity atoms in the pore wall, which is inherent in real systems, may nevertheless have a substantial effect on the domain growth. An average over many isolated pores corresponding to an assembly of noninterconnected (unlike Vycor) pores, as we consider it in this paper, was experimentally realized[14] by a B-doped Si wafer via electrochemical etching.

The structure of the paper is as follows. In Sec. II we define the model and describe the Monte Carlo technique that we have used in our simulation. In Sec. III A, we discuss the hysteresis phenomena for different pore geometries in two and three dimensions and discuss how one can differentiate the pore structure from the hysteresis loops. In Sec.

[a]Electronic mail: paul@lusi.uni.-sb.de

 © 2005 American Institute of Physics

Downloaded 25 Jul 2005 to 134.96.30.62. Redistribution subject to AIP license or copyright, see http://jcp.aip.org/jcp/copyright.jsp

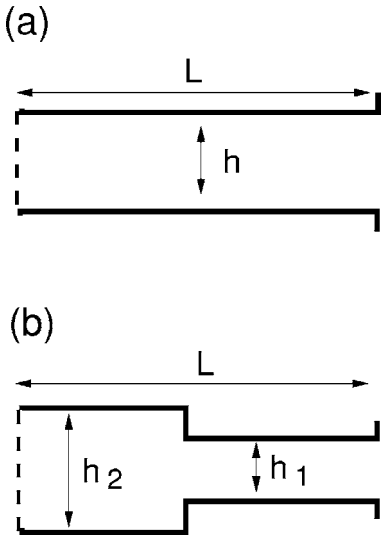

FIG. 1. Schematic representation of (a) simple pore and (b) ink-bottle pore. The dotted line is due to the fact that the pore may by open from both ends.

III B, we focus on the evaporation of particles from the pore and discuss how the density in the pore reaches a new equilibrium value. Section III C and III D are entirely devoted to the domain evolution in the pore environment where we propose a random-walk picture of the domain growth above a critical size comparable to the pore diameter. Then we perform a quantitative study of the growth phenomenon for a simple pore as well as for pores with defects. Finally Sec. IV finishes the paper with a discussion.

II. SIMULATION MODEL

A standard model for a binary liquid mixture is the Ising lattice-gas model with spin occupancy variables $\sigma_i=0$, 1 governed by the Hamiltonian:

$$\mathcal{H} = -W_{\mathrm{pp}} \sum_{\mathrm{bulk}\langle i,j\rangle} \sigma_i\sigma_j - W_{\mathrm{wp}} \sum_{i\ \mathrm{n.n.\ of\ wall}} \sigma_i, \tag{1}$$

where W_{pp} and W_{wp} are the particle-particle and wall-particle couplings, respectively. We denote an occupied site as a particle and an empty site as a vacancy. Experimental observations suggest that in the case of a glass (Si) adsorbent, the pore wall has a very strong affinity towards the adsorbed gases, which implies $W_{\mathrm{wp}} > W_{\mathrm{pp}}$. Most of our simulations, unless otherwise specified, are performed at a fixed "wettability" $W_{\mathrm{wp}}/W_{\mathrm{pp}}=1.5$. A change in this value does not qualitatively affect our results as long as $W_{\mathrm{wp}} > W_{\mathrm{pp}}$. The geometry of the simple pore [see Fig. 1(a)] is chosen to be a rectangle of size $L\times h$ in two dimensions and parallelepiped of size $L\times h\times h$ in three dimensions with $h \ll L$. An ink-bottle pore [see Fig. 1(b)] consists of two simple pores of unequal radii h_1 and h_2. Standard-conserved order-parameter dynamics (Kawasaki) is employed to study the diffusion and the domain growth kinetics in the nanopores. A spin σ_i at site i chosen randomly and exchanged with one of its nearest-neighbor spin σ_j at site j, with Metropolis acceptance probability

$$P(\{\sigma\} \to \{\sigma'\}) = \min[1, \exp(-\beta\mathcal{H}\{\sigma'\})/\exp(-\beta\mathcal{H}\{\sigma\})], \tag{2}$$

where σ and σ' represent the old and new spin configurations, respectively. In order to avoid ineffective exchange moves between empty sites we make a list of all occupied sites (particles) and choose update sites randomly from this list. The selected site is then exchanged with a randomly chosen nearest neighbor according to Eq. (2). One Monte Carlo (MC) step contains a number of trial updates which is equal to the total number of particles actually present in the system.

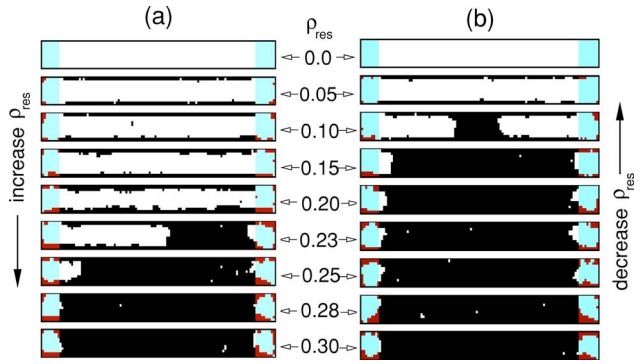

FIG. 2. Snapshots of the hysteresis in a simple nanopore of size $L=100$ and $h=11$ at temperature $T=0.3$. The shaded regions and the black spots on both sides of the pore are, respectively, the attached reservoirs and the particles in it. For each value of ρ_{res} the system is equilibrated up to $t=2^{22}$. Snapshots (a) correspond to the adsorption and (b) correspond to the desorption isotherms.

III. NUMERICAL RESULTS

A. Hysteresis

To study hysteresis in the adsorption/desorption process within a pore we attach one or two reservoirs depending upon the geometry of the pore. To avoid asymmetric diffusion into the pore, no periodic boundary condition is applied between the reservoirs. The particle density in the reservoirs is kept constant by adding (removing) a particle at a randomly chosen position in the reservoir as soon as a particle diffuses into the pore (reservoir). A snapshot of the hysteresis phenomenon for a simple pore geometry in $2d$ is shown in Fig. 2. Initially, both the pore and the reservoirs are kept empty. The density of particles in the reservoirs (ρ_{res}) are then slowly increased. Particles are immediately adsorbed and form a single layer along the pore walls. At this stage the density in the pores (ρ_f) rises sharply to a nonzero value which corresponds to the first jump of adsorption isotherms (Fig. 3). Then ρ_f forms a long plateau until two semicircular (or hemispherical in $3d$) meniscii (a meniscus for one-end open pore) are formed somewhere in the middle of the pore at a high-reservoir density and move apart from each other to fill the entire pore; a second jump in ρ_f is observed. We call this complete pore filling and further increase in ρ_{res} does not change ρ_f.

Downloaded 25 Jul 2005 to 134.96.30.62. Redistribution subject to AIP license or copyright, see http://jcp.aip.org/jcp/copyright.jsp

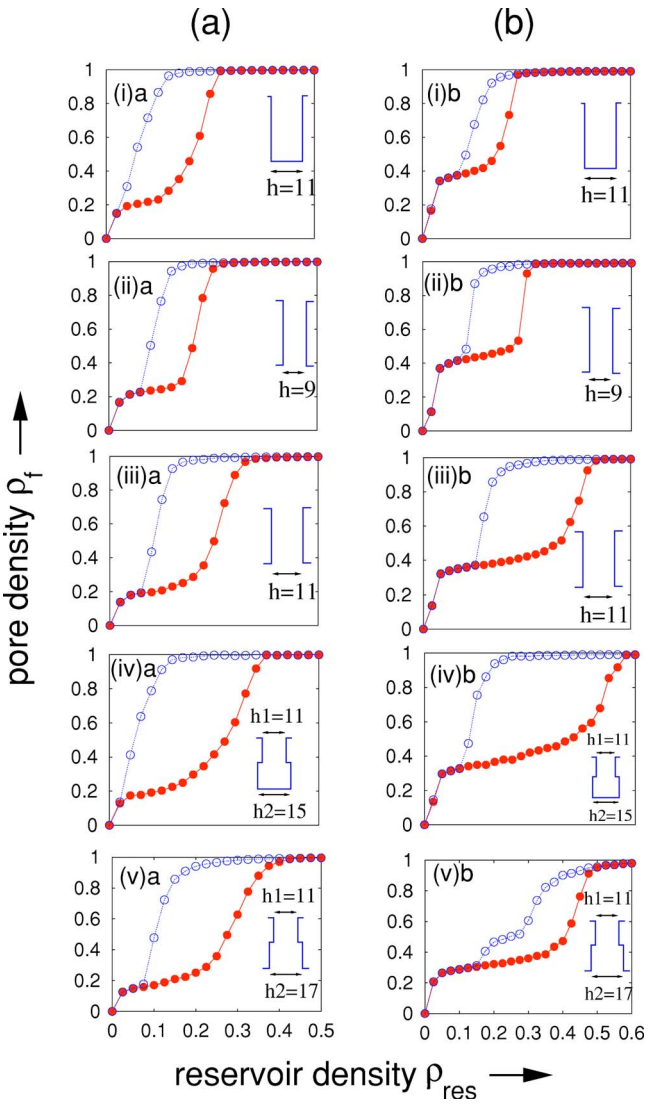

FIG. 3. Adsorption (filled circles) and desorption (empty circles) isotherms for nanopores. (a) Filling fraction ρ_f of the pore as a function of the reservoir density ρ_{res} in two dimensions. The equilibration time t_w for each data point 2^{22}. (a)(i) has one reservoir of length 10 attached to the open end. (a)(ii), (a)(iii), and (a)(iv) have two reservoirs attached on both sides. (b) Hysteresis isotherms in three dimensions. Equilibration time $t_w=2^{22}$, pore length $L=50$, and reservoir length is 10. For each hysteresis isotherm, data are averaged over 50 disorder samples.

Next, we slowly decrease the reservoir density and record the corresponding filling fraction ρ_f after the system is equilibrated. On desorption, however, at a much smaller reservoir density ρ_{res}, we see the semicircular meniscii to form on the open ends of the pore, followed by a sharp fall in the pore density ρ_f, as the meniscii approach towards each other. Finally the desorption curve follows the same path as that of the adsorption. Since the diffusion into the pores is very slow, a long waiting time t_w is needed to equilibrate the whole system for each value of ρ_{res}.

Our simulation results are shown in Fig. 3 where the columns (a) and (b) show the hysteresis in two and three dimensions, respectively. The simulations are performed with systems of length $L=100$ and 50 at temperatures $T=0.3$ and 0.6 in $2d$ and $3d$, respectively. Reservoir lengths are kept fixed at $L_r=10$. The ink-bottle pores are equally divided into two parts, one with the narrow tube of diameter h_1 and the other is a relatively wider sack with diameter h_2. To make sure that pore density ρ_f does not change anymore, each data point of the sorption isotherms is equilibrated for $t_w=2^{22}$ time steps. Finally for each hysteresis loop, data are averaged over 50 ensembles. It is evident from the sorption branches of Figs. 3(a)(i)–3(a)(iii) and 3(b)(i)–3(b)(iii) that they are much steeper than in Figs. 3(a)(i) and 3(b)(i). This is due to the formation of two meniscii on both sides of the pore, which accelerate the filling and emptying procedures. Such characteristic feature distinguishes between a one-end open and both-end open pores. Further, an increase in pore diameter requires a higher-reservoir density to initiate the formation of meniscii, which effectively delays the onset of adsorption saturation. As a result the loop area for a bigger pore is also increased as shown in Figs. 3(a)(ii) and 3(b)(ii) and 3(a)(iii) and 3(b)(iii). These features can be used to compare pores of different sizes.

Experimentally[14] one observes a two-step decrease of the desorption isotherms for ink-bottle pores. Our data, as shown in Fig. 3(b)(v), for a both-end open pore in $3d$ of similar geometry agrees with this experimental observation. The two-step decrease of the desorption isotherm arises from the sequential emptying of the different sections (of diameter h_1 and h_2) of the pore. The heights of the two steps suggest that the wider section of the pore emptied earlier than the smaller section. However, the one-end open ink-bottle geometry [Fig. 3(b)(iv)] does not show this two-step feature, in contrast with the experimental finding.[14] There the two-step feature for ink-bottle pores vanishes only for much smaller temperatures, when the adsorbent is already in the solid phase. Since the temperature is equal in Figs. 3(b)(iv) and 3(b)(v) a possible reason for the discepancy we found could be that our system sizes and the ratio h_2/h_1 are too small to detect this feature. In $2d$ ink-bottle pores we do not observe a two-step process at all, neither when only one end is open [Fig. 3(a)(iv)] nor when both ends are open [Fig. 3(a)(v)].

B. Evaporation

If a partially or completely filled pore is kept in vacuum, the density inside it decreases with time. This is what we call evaporation, and we investigate it for different pore geometries. In experiments[14] one measures the vapor pressure change inside a previously equilibrated pore subject to the pressure variation in the reservoir. However, we carry out the simulation in a slightly different way by keeping the initial pore density just above the desorption threshold.

To study the variation in pore density ρ_f as a function of time we fill pores completely and allow it to evaporate in an empty reservoir (vacuum). The change in ρ_f has been recorded as a function of time t. The decay of the pore density can be very well described by a stretched exponential law,

$$\rho_f(t) \sim \exp[-(t/\tau)^{\beta}]. \tag{3}$$

The simulations are carried out for pores with both simple and ink-bottle geometries. For simple pore we study the evaporation at temperature $T=0.4$, for systems with $L=128$, 256, 400, and 512 and $h=7$ and finally average over 50 en-

Downloaded 25 Jul 2005 to 134.96.30.62. Redistribution subject to AIP license or copyright, see http://jcp.aip.org/jcp/copyright.jsp

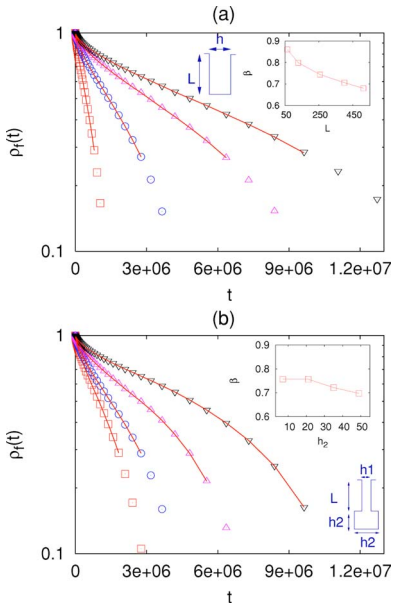

FIG. 4. (a) Evaporation from simple pores of diameter $h=7$ and different lengths $L=128$, 256, 400, and 512 from left to right at temperature $T=0.4$. The data for the filling fraction $\rho_f(t)$ are shown in a log-linear scale—note that the decay is initially slower than exponential. The full line connects the data points that can very well be fitted to a stretched exponential with the exponent β given in the inset. Inset: The decay exponent β as a function of the pore length L. (b) $\rho_f(t)$ for ink-bottle pores of fixed length $L=200$ and tube diameter $h_1=7$ at $T=0.4$ for different sack widths of $h_2=7$, 21, 25, and 49 from left to right. The decay law is similar to the simple pores. Inset: β as a function of h_2.

sembles. The pore density ρ_f as a function of time t is plotted in Fig. 4(a) in a log-linear scale. It is noticed that a pure stretched exponential decay is found only above a certain value of the pore filling fraction as shown by continuous lines. These values of ρ_f are nothing but the ratio between the number of surfaces to bulk molecules and decreases as L becomes larger. The surface molecules are attached rather strongly ($W_{wp} > W_{pp}$) to the walls and slow down the evaporation rate for a while but finally drop off suddenly to zero. As the length of the system is increased, the particles deep inside the pore require much more trial attempts to diffuse till the open end which effectively increases the evaporation time for longer pores. This leads to the decay exponent β to decrease with L, as shown in the inset of (a).

A similar study in the case of ink-bottle pores was carried out with systems of fixed $L=200$ and $h_1=7$ for different values of $h_2=7$, 21, 35, and 49 as shown in Fig. 4(b). The temperature is kept fixed at $T=0.4$ and data are averaged over 50 ensembles. Like the previous case, here also, ρ_f shows a pure stretched exponential decay above a certain value, which becomes smaller as h_2 is increased. Moreover the effective length $(L+h_2)$ of the pore increase with h_2 results in the decay exponent β [inset of (b)] to drop off similarly to the simple pore. A further analysis (not shown) on both simple and ink-bottle pores show that β is independent of the temperature.

C. Domain evolution and random walks

In this section we study the temporal evolution of domain structures inside pores starting with a random (high temperature) initial configuration of given density. Now we use periodic boundary conditions between the two ends of the pore and the total number of particles is conserved. Figure 5(a) shows the domain structure profile at different time steps when the system is quenched $T=0.3$ $T=\infty$. Figure 5(b) is the snapshot of a cut along the pore axis. The black regions correspond to the occupied sites and are called "particle domains," whereas empty white regions are termed "blobs."

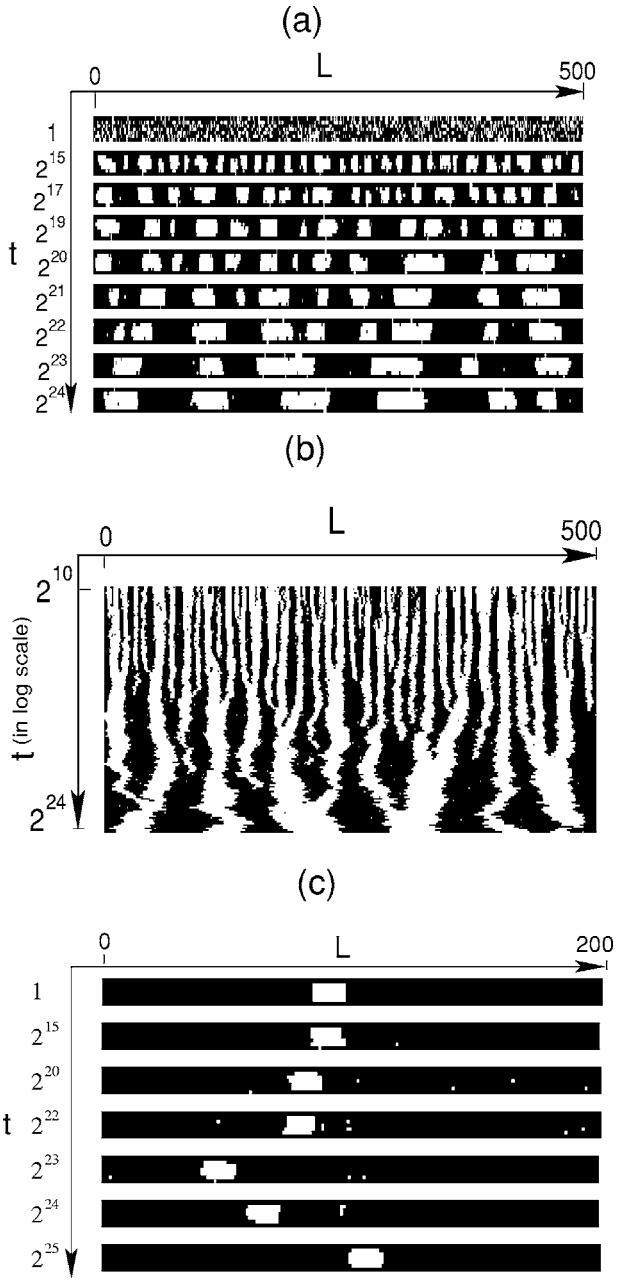

FIG. 5. (a) Domain evolution in nanopores. The figures are produced by taking a snapshot for a system of length $L=300$ and height $h=7$ at temperature $T=0.3$. (b) Axial snapshot of the domains for the same system in (a). A horizontal cut through the figure at any instant t will give the location and size of domains/blobs along the axis of the pore. The time is plotted in logarithmic scale. (c) Time evolution of a single rectangular blob of linear size $l_b=13$ in a pore of dimension 200×7 at $T=0.3$.

In the initial stage, the growth is dominated by nucleation and spinodal decompositions. As soon as the domain or

Downloaded 25 Jul 2005 to 134.96.30.62. Redistribution subject to AIP license or copyright, see http://jcp.aip.org/jcp/copyright.jsp

the blob size becomes comparable to the diameter of the pore, the above two mechanisms do not work anymore. Transverse directional growth is completely stopped because of the pore wall and the horizontal movement of the blobs is slowed down by the presence of the particle domains.

The snapshots in Fig. 5 confirm that the random motion of the blobs plays an important role in the late stage of growth. A closer look to Fig. 5(b), which is horizontally the occupancy along the pore axis and vertically the time in log scale, shows in the late stage that the blobs move to and fro along the axis of the pore and penetrate through the particle domains to coalesce with the neighbors. During this process it also transfers holes (vacancies, white regions) from its surface to the neighboring blobs.

To elucidate the random motion, we study the time evolution of a single blob as shown in Fig. 5(c). Initially it is a perfect rectangle of linear size (l_b) comparable to the pore diameter (h) and placed in the center of the pore. The temperature is kept fixed at $T=0.3$. The system is allowed to evolve and the mean-square deviation $\langle x^2(t)\rangle$ of the center of mass (COM) of the blob along the axis of the pore is measured at each time step. Since the boundary of the blob perpendicular to the wall fluctuates very rapidly, the true COM may not lie on the geometrical axis of the pore. In this case we trace the actual COM and project it on to the axis. The size of the blob has to be chosen large enough to avoid disintegration of the main blob.

Since we start with an exactly rectangular blob, a true random-walk motion is not immediately observed. In the early stages, the blob walls perpendicular to the pore axis roughens, leading to $\langle x^2(t)\rangle \sim t^{2/3}$ as in surface roughening described by the Kandar-Parisi-Zhang (KPZ) equation.[25] At late stages ($t > 10^4$), the blob performs a random walk with a blob-size-dependent diffusion constant $\mathcal{D}(l_b)$,

$$\langle x^2(t)\rangle = \mathcal{D}(l_b)t. \tag{4}$$

Figure 6(a) shows the mean-square displacement $\langle x^2(t)\rangle$ of the COM of blobs with $l_b=11$, 15, 19, 23, 27, 31, 35, and 39 as a function of time t. For each values of l_b the simulation is carried out in a system with fixed $L=200$ and $h=7$ at temperature $T=0.3$, and finally averaged over 1000 ensembles. It is evident from the figure that the onset of a true random walk is delayed for bigger blobs. A scaling form for both small and large time scale regimes is

$$\langle x^2(l_b,t)\rangle \propto \tau^{\theta}(l_b) f(t/\tau(l_b)), \tag{5}$$

with

$$f(x) \sim \begin{cases} x^{\theta}, & \text{for } x \ll 1, \\ x, & \text{for } x \gg 1. \end{cases} \tag{6}$$

Assuming $\tau(l_b) \sim l_b^{\,z}$ from Eq. (5), one can write for large time $t \gg \tau$,

$$\langle x^2(l_b,t)\rangle \propto l_b^{\,z(\theta-1)} t, \tag{7}$$

which readily gives

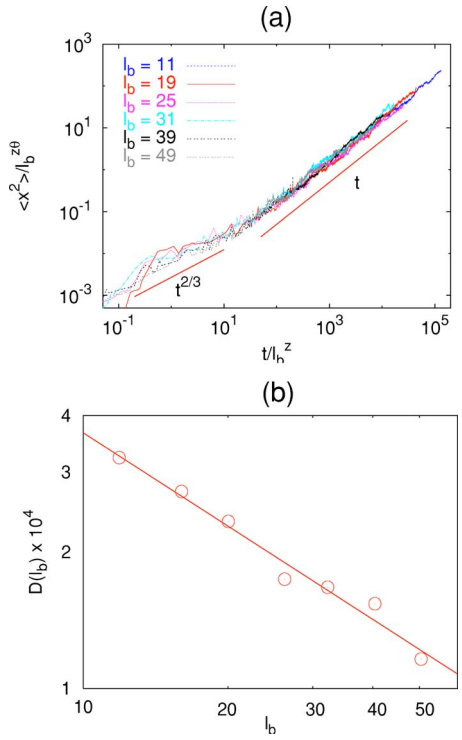

FIG. 6. (a) Mean-square deviation of blobs of size $l_b=11$, 15, 19, 23, 27, 31, 35, and 39 for a system size are $L=200$ and $h=7$ and the temperature $T=0.3$. (b) The power-law decay of the diffusion constant $\mathcal{D}(l_b)$ for different blob sizes. The exponent is found to be $\gamma=0.68$.

$$\mathcal{D}(l_b) \sim l_b^{-z(1-\theta)} = l_b^{-\gamma}. \tag{8}$$

The scaling form in Eq. (5) gives quite reasonable data collapse for $\theta=2/3$ and $z=2$, as shown in Fig. 6(a). Substituting these values in Eq. (8) we obtain the value of $\gamma=2/3$. The diffusion constant $\mathcal{D}$ evaluated from the asymptotic behavior [cf. Fig. 6(a)] is plotted in Fig. 6(b). From the slope of $\mathcal{D}$ vs l_b curve in log-log scale we estimate the $\gamma=0.68$ which agrees quite well with the previous value 2/3, obtained from the scaling. Note that the relation $\mathcal{D} \propto 1/l_b^{2/3}$ deviates from the naive expectation $\mathcal{D} \propto k_B T\eta/l_b$,[22,26] where k_B, T, and η are the Boltzmann's constant, temperature, and viscosity coefficient of the medium, respectively.

D. Correlation function and domain growth exponent

An alternative way to study domain growth is via the measurement of the correlation function $C(r,t)$ along the axis of the nanopore in a similar fashion as in the Ising model.

$$C(r,t) = \langle S(0,t)S(r,t)\rangle - \langle S\rangle^2, \tag{9}$$

where $S(r,t)=2\sigma(r,t)-1$, the lattice-gas variable, takes the values -1 and 1 for $\sigma=0$ and 1, respectively. Due to this transformation, $C(r,t)$ falls off with r in an oscillatory fashion, as is shown in the inset of Fig. 7(a). Following Huse,[27] we also define the length scale or the typical domain size $R(t)$ of the system as the position of the first zero of $C(r,t)$. Calculating $C(r,t)$ using Eq. (9) we extract $R(t)$ by fitting the three or four points in $C(r,t)$ closest to its first zero to a quadratic function of r and defining $R(t)$ as the value of r for which the function vanishes. At very late stage [$t > \tau(T)$], the

Downloaded 25 Jul 2005 to 134.96.30.62. Redistribution subject to AIP license or copyright, see http://jcp.aip.org/jcp/copyright.jsp

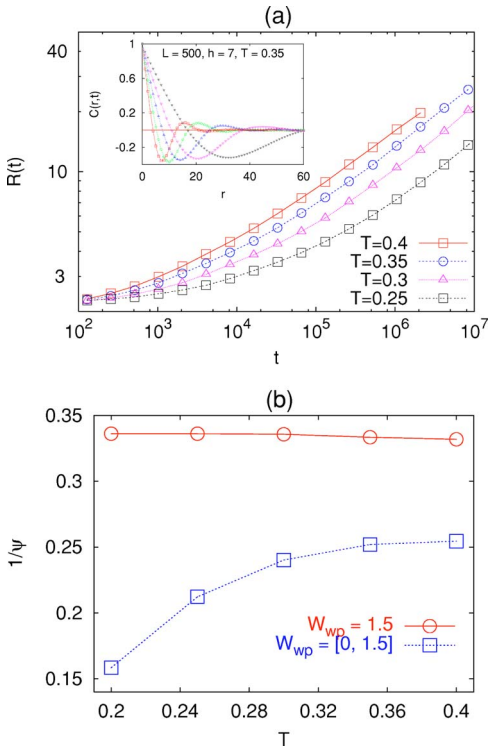

FIG. 7. (a) Average domain size $R(t)$ as a function of time t for different quenches to $T=0.4$, 0.35, and 0.3. The system size are $L=500$ and $h=7$ and the density $\rho_f=0.7$. Inset: Correlation function $C(r,t)$ at various times t after a quench to $T=0.35$. The domain size $R(t)$ is defined as the distance of the first zero from the origin. (b) Growth exponent $1/\psi$ plotted against the temperature T. The upper curve, for fixed W_{wp}, is almost a constant with T, whereas the lower one, for random W_{wp}, shows a steep decrease for smaller values of T.

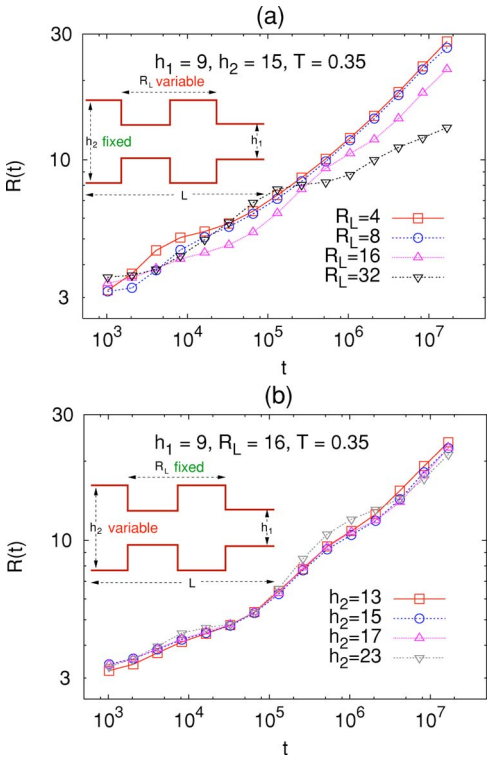

FIG. 8. (a) Average domain size $R(t)$ of a defected pore wall for periodicities $R_L=4$, 8, 16, and 32 at temperature $T=0.35$. The system has fixed length $L=512$ and diameters $h_1=9$ and $h_2=15$. The domain growth slows down for larger periodicity. (b) $R(t)$ for different pore diameters $h_2=13$, 15, 17, and 23 at fixed $L=512$, $h_1=9$, $R_L=16$, and $T=0.35$. The domain growths remain constant while varying h_2.

asymptotic domain size $R(t)$ grows as a power law,

$$R(t) \sim t^{1/\psi}, \tag{10}$$

where $1/\psi$ is the growth exponent. The onset of such a power-law regime shifts towards the early time scales as the temperature is increased.

We studied the domain growth for both (i) simple and (ii) complex pores. By "simple" we specify a pore with no geometrical defects in the wall and has a fixed value of W_{wp}. "Complex" pores are further subcategorized into (ii)-A, simple pore with random $W_{\mathrm{wp}} \in [0,1.5]$, and (ii)-B, pore with fixed W_{wp} but geometrical defects along the wall. Let us discuss the simple pores first. The domain evolution in this case studied with a system of length $L=500$ and height $h=7$ at different temperatures of $T=0.25$, 0.3, 0.35, and 0.4. For each temperature we averaged over 300 ensembles. The average length scale or the domain size $R(t)$ as a function of the time t is plotted in Fig. 7(a). The growth exponents $1/\psi$, extracted from this figure, for different values of temperatures, are shown by the upper curve in Fig. 7(b). This exponent appears to be $1/\psi \sim 1/3$ independent of the temperature. On the other hand, for the case (ii)-A with defects in terms of random wall-particle coupling $W_{\mathrm{wp}} \in [0,1.5]$, we carried out a similar kind of study as described above. It is observed that the growth process is drastically slowed down by the pinning effect[28] of nonwetting sites located randomly in the pore walls. And as a consequence the exponents are also reduced quite significantly and found to have a temperature dependence as well, as shown in the bottom of Fig. 7(b).

It is also noticed, for the case (ii)-B, that a periodic structure defect of the pore wall has a strong influence on the domain growth. In Fig. 8(a) we demonstrate the effect of a variable periodicity R_L for system of length $L=512$ with two fixed pore diameters $h_1=9$ and $h_2=15$. The simulations are done at a constant temperature $T=0.35$ and for each value of R_L, the data are averaged over 300 ensembles. Domains grow quite fast in either part of the h_1 or h_2 diameter, but finally due to the bottle-neck effect it becomes extremely hard to transfer the particle domains or blobs from one side of the narrow part (diameter h_1) of the pore to the other. Consequently the growth process is slowed down. But in the late stage, when the domain size $R(t)$ becomes comparable to the periodicity R_L, the blobs are in a similar environment such as in a simple pore and a true power-law growth sets on. As a result a longer periodicity corresponds to a late initiation of the power-law growth. We carried out the simulation for four different values of periodicity $R_L=4$, 8, 16, and 32 and for the first three values of R_L we found a late-stage growth exponent $1/\psi=0.33$, but for $R_L=32$, the power-law growth is not yet initiated. For such a large periodicity one certainly has to wait extremely long. Further, we carried out a similar study by varying the pore diameter h_2 while keeping the periodicity R_L fixed. The numerical data are obtained with a system of $L=512$, $h_1=9$, R_L, $T=0.35$, and $h_2=13$, 15, 17, and 23. Finally for each value h_2 we average

Downloaded 25 Jul 2005 to 134.96.30.62. Redistribution subject to AIP license or copyright, see http://jcp.aip.org/jcp/copyright.jsp

over 300 ensembles. The domain size $R(t)$ is plotted in Fig. 8(b). In the initial stage of the growth, as described above, the domain grows quite independently in either part of the pore with h_1 and h_2 diameters. A true power-law growth, which starts after $R(t) \geqslant R_L$, is slightly delayed for larger h_2. As described above, to attain a pore environment similar to the simple pore it is necessary to equilibrate the top and bottom of the wider part (h_2) of the pore which takes longer as h_2 is increased. Finally, the growth exponent extracted in the late stage was found to have the same value $1/\psi = 0.33$, as that of the pure model.

IV. DISCUSSION

Using extensive Monte Carlo simulations we have shown how hysteresis arises in nanopores for different pore structures. The characteristics of the sorption branches are influenced by the shape and size of the pore geometry. Since the hysteresis in nanopores occur due to diffusion, the temperature has to be chosen very carefully to avoid a slow diffusion rate at low temperatures or a vanishing hysteresis loop at high temperatures. The absence of a two-step desorption branch in $2d$ ink-bottle pores may be due to the effect of a small temperature as found in the experiment.[14] The choice of the pore diameters for one-end open ink-bottle geometry is also an important factor. Because of the surface-tension effect, a large curvature ratio $(1/h_1)/(1/h_2)$ can cause a huge pressure difference between the narrow and wide parts of the pore. The increase in curvature corresponds to a decrease in vapor pressure, described by the Kelvin equation. As an effect if the narrow part of the pore is filled early, it can block the particle to diffuse into the wider part, unless a very high density is reached in the reservoir.

The stretched exponential decay of the pore density $\rho_f(t)$ also agrees qualitatively with the experiments.[14] One simple reason of such a behavior of $\rho_f(t)$ could be due to the formation of a meniscus at the open end of the pore which eventually restricts the rate of evaporation depending upon the radius of its curvature.

For the phase separation of binary liquids in the pore environment, model B, (Ref. 29) corresponding to dynamics with conserved order parameter, is not well suited, as it does not account for the transport of the order parameter by hydrodynamic flow. Modifications to model B by adding an "advection" term describes the system quite well.[30]

The late-stage coarsening in the pore system that we studied is effectively driven by two mechanisms: (1) The transfer of holes from the surface of one blob to a neighboring blob and (2) the transfer of particles from one side of the blob to the other along the pore wall. Owing to the first mechanism a blob shrinks and the neighboring blobs grow, whereas due to the second one a blob moves to and fro as a whole and coalesce with another. Our numerical study for a single blob [Sec. III C] accounts for the contribution arising from (2) only and gives rise to the diffusion constant $\mathcal{D} \sim l_b^{-2/3}$ of a blob of size l_b. The first mechanism modifies the single-blob diffusion constant in a nontrivial way, which is difficult to estimate. Finally, the superposition of random motion of blobs due to mechanism (2) and the hole transfer mechanism in (1) leads to a late-stage growth law $R(t) \sim t^{1/3}$, independent of their individual contributions.

The domain growth exponent $1/\psi$ is significantly decreased in the presence of random wall-particle potential W_{wp} which in practice is due to the effect of impurity atoms at the pore walls. The temperature dependence of the exponent may come from a logarithmic scaling[29] of the barrier energy of the domains. On the other hand geometrical defects appear to slow down the growth process only in the early time regime. But in the late stage, as the blob size becomes larger than the wavelength of the geometrical disorder, which in this case is the periodicity of the wall defect, the domain growth displays the same behavior as in the case of smooth walls.

ACKNOWLEDGMENT

This work was financially supported by the Deutsche Forschungsgemeinschaft (DFG), SFB277.

[1] F. Rouqerol, J. Rouqerol, and K. Sing, *Adsorption by Powders and Porous Solids* (Academic, New York, 1999), Chap. 7.
[2] K. S. W. Sing, D. H. Everett, R. A. W. Haul, L. Moscou, R. A. Pierotti, J. Rouqerol, and T. Siemieniewska, Pure Appl. Chem. **57**, 603 (1985).
[3] L. D. Gelb, K. E. Gubbins, R. Radhakrishnan, and M. Sliwinska-Bartkowiak Rep. Prog. Phys. **62**, 1573 (1999).
[4] D. H. Everett, in *The Solid Gas Interface*, edited by E. A. Flood (Marcel Dekker, New York, 1967), Vol. 2, p. 1055.
[5] W. F. Saam and M. W. Cole, Phys. Rev. B **11**, 1086 (1975).
[6] F. Celestini, Phys. Lett. A **228**, 84 (1997).
[7] A. Papadopoulou, F. van Swol, and U. Marini Bettolo Marconi, J. Chem. Phys. **97**, 6942 (1992).
[8] R. Evans, U. Marini Bettolo Marconi, and P. Tarazona, J. Chem. Phys. **84**, 2376 (1986).
[9] R. A. Guyer and K. R. McCall, Phys. Rev. B **54**, 18 (1996).
[10] G. Mason, Proc. R. Soc. London, Ser. A **415**, 453 (1988).
[11] L. Sarkisov and P. A. Monson, Langmuir **17**, 7600 (2001) and references therein.
[12] J. H. Page, J. Liu, B. Abeles, H. W. Deckman, and D. A. Weitz, Phys. Rev. Lett. **71**, 1216 (1993).
[13] P. Huber and K. Knorr, Phys. Rev. B **60**, 12657 (1999).
[14] D. Wallacher, N. Künzner, D. Kovalev, N. Knorr, and K. Knorr, Phys. Rev. Lett. **92**, 195704 (2004).
[15] D. Stauffer and R. B. Pandey, J. Phys. A **25**, L1079 (1992).
[16] M. C. Goh, W. I. Goldburg, and C. M. Knobler, Phys. Rev. Lett. **58**, 1008 (1987).
[17] S. B. Dierker and P. Wiltzius, Phys. Rev. Lett. **58**, 1865 (1987).
[18] M. Y. Lin, S. K. Sinha, J. M. Drake, X.-l. Wu, P. Thiyagrajan, and H. B. Stanley, Phys. Rev. Lett. **72**, 2207 (1994).
[19] F. Brochard and P. G. de Gennes, J. Phys. (Paris), Lett. **44**, 785 (1983).
[20] P. G. de Gennes, J. Phys. Chem. **88**, 6469 (1984).
[21] R. J. Birgeneau, R. A. Cowley, G. Shirane, and H. Yosthizawa, J. Stat. Phys. **34**, 817 (1984).
[22] L. Monette, A. J. Liu, and G. S. Grest, Phys. Rev. A **46**, 7664 (1992);A. J. Liu, D. J. Durian, E. Herbolzheimer, and S. A. Safran, Phys. Rev. Lett. **65**, 1897 (1990).
[23] I. M. Lifshitz and V. V. Slyozov, J. Phys. Chem. Solids **19**, 35 (1961).
[24] J. C. Lee, Phys. Rev. B **46**, 8648 (1992).
[25] M. Kardar, G. Parisi, and Y. C. Zhang, Phys. Rev. Lett. **56**, 889 (1986).
[26] E. D. Siggia, Phys. Rev. A **20**, 595 (1979).
[27] A. J. Bray, Adv. Phys. **51**, 481 (2002).
[28] D. A. Huse, Phys. Rev. B **36**, 5383 (1987).
[29] R. Paul, S. Puri, and H. Rieger, Europhys. Lett. **68**, 881 (2004).
[30] P. C. Hohenberg and B. I. Halperin, Rev. Mod. Phys. **49**, 435 (1977).

Downloaded 25 Jul 2005 to 134.96.30.62. Redistribution subject to AIP license or copyright, see http://jcp.aip.org/jcp/copyright.jsp